REPORT DOCUMENTATION PAGE

Form Approved
OMB No. 0704-0188

PLEASE DO NOT RETURN YOUR FORM TO THE ABOVE ORGANIZATION.

1. REPORT DATE *(DD-MM-YYYY)*	2. REPORT TYPE	3. DATES COVERED *(From - To)*
19-03-2011	Final Report	01-08-2008 - 31-11-2010

4. TITLE AND SUBTITLE
TRANSIENT BOUNDARY LAYER DISTURBANCE GROWTH & BYPASS TRANSITION DUE TO REALISTIC ROUGHNESS & CONTINUED STUDY OF TRANSITION OVER RIBLETS

5a. CONTRACT NUMBER

5b. GRANT NUMBER
FA9550-08-1-0453

5c. PROGRAM ELEMENT NUMBER

6. AUTHOR(S)
David B Goldstein

5d. PROJECT NUMBER

5e. TASK NUMBER

5f. WORK UNIT NUMBER

7. PERFORMING ORGANIZATION NAME(S) AND ADDRESS(ES)
The University of Texas at Austin
Austin, TX 78712

8. PERFORMING ORGANIZATION REPORT NUMBER

9. SPONSORING/MONITORING AGENCY NAME(S) AND ADDRESS(ES)
Air Force Office of Scientific Research
875 North Randolph Street
Suite 325, Rm 3112
Arlington, VA 22203

10. SPONSOR/MONITOR'S ACRONYM(S)
AFOSR

11. SPONSOR/MONITOR'S REPORT NUMBER(S)
AFRL-OSR-VA-TR-2012-0288

12. DISTRIBUTION/AVAILABILITY STATEMENT
Public Distribution-A

13. SUPPLEMENTARY NOTES

14. ABSTRACT

In this two part study we worked on surface texturing for turbulent boundary layer control and on a collaborative effort with Ed White to understand how surface roughness induces boundary layer transition. Streamwise textures including triangular riblets and fins were explored in an effort to inhibit the spanwise spreading of turbulent spot/wedge disturbances. Appreciable care has been taken in examining the meaning of spreading angle. We have concentrated on the mechanisms of lateral spreading of the regions of turbulence. Since we use DNS in our work, we have been able to utilize a range of tricks, unavailable in a physical experiment, in an attempt to tease out the causes of lateral spreading of spots. In a parallel effort, we have concentrated on matching results from previous DNS done by Rizetta and Visbal and experiments done by White for flow over an array of tiny cylindrical perturbations. In an effort to understand the differences we have conducted some simple flow visualization and LDA surveys in the UT water channel and have examined in detail the vorticity dynamics about the perturbation. We have also demonstrated agreement between our DNS of laminar flow over distributed roughness patches and the TAMU experiments.

15. SUBJECT TERMS

16. SECURITY CLASSIFICATION OF:			17. LIMITATION OF ABSTRACT	18. NUMBER OF PAGES	19a. NAME OF RESPONSIBLE PERSON
a. REPORT	b. ABSTRACT	c. THIS PAGE		21	David B Goldstein
					19b. TELEPHONE NUMBER *(Include area code)* 512-471-4187

Reset

Transient Boundary Layer Disturbance Growth and Bypass Transition Due to Realistic Roughness and Continued Study of Transition Over Riblets

Final report for grant: FA 9550-08-1-0453 for the period 8/1/08-11/31/10

David Goldstein

Center for Aeromechanics Research
Department of Aerospace Engineering and Engineering Mechanics
The University of Texas at Austin
Austin, TX 78712

Abstract:
In this two part study we worked on surface texturing for turbulent boundary layer control and on a collaborative effort with Ed White to understand how surface roughness induces boundary layer transition. Streamwise textures including triangular riblets and fins were explored in an effort to inhibit the spanwise spreading of turbulent spot/wedge disturbances. Appreciable care has been taken in examining the meaning of spreading angle. We have concentrated on the *mechanisms* of lateral spreading of the regions of turbulence. Since we use DNS in our work, we have been able to utilize a range of tricks, unavailable in a physical experiment, in an attempt to tease out the causes of lateral spreading of spots. In a parallel effort using the same DNS code, we have concentrated on matching results from previous DNS done by Don Rizetta and Miguel Visbal and experiments done by Ed White for flow over an array of tiny cylindrical perturbations. We can generally match the experiments and earlier CFD but we find somewhat different details. In an effort to understand the differences we have conducted some simple flow visualization and LDA surveys in the UT water channel and have examined in detail the vorticity dynamics about the perturbation. We have also demonstrated agreement between our DNS of laminar flow over distributed roughness patches and the TAMU experiments and highlighted the origin of flow structures in the wake.

Background:
A greater knowledge of transitional and turbulent boundary layer structures, their development, and the creation of means for boundary layer control are essential to numerous applications in aerodynamics, particularly in the area of drag reduction. Critical features of the transition process from a laminar to a turbulent boundary state occur among small scale flow structures near the solid wall. It is possible to directly simulate transitional and turbulent flow about modestly complex boundary geometries using the full Navier Stokes equations to elucidate the interactions among the turbulent flow structures and the wall.

Turbulent Spots and Wedges: As Tollmien-Schlichting waves or other disturbances in a boundary layer grow to large amplitudes, secondary instabilities develop and turbulent spots form. Such arrowhead-shaped spots appear at randomly distributed points and their growth and merging lead to complete transition to turbulence. A spot appears as a fairly well defined region of turbulence surrounded by laminar flow. Wygnanski et al (1976, and their later work), performed detailed experimental studies of such. Spots have been successfully

simulated in several shear flows (e.g., Singer and Joslin, 1994, Henningson et al., 1987). Spots appear to displace some near-wall fluid outward (a spanwise velocity component) and produce oblique traveling waves (Tillmark, 1995).

While the process of spot development and growth can be observed and described in the well-controlled conditions that lead to a T-S-dominated transition scenario, flow conditions are often not sufficiently perfect that transition occurs via this path. Roughness elements can cause an immediate bypass transition to turbulence in a wedge-like region. We note that in both the formation of turbulent spots and wedges, the near-wall turbulent structures of streamwise vortices and hairpins appear much like those in a fully developed turbulent boundary layer. In fact, the lateral spread with downstream propagation distance of those spots/wedges appears related to those same fundamental structures.

Delaying Transition With Surface Textures: If one could delay or eliminate the onset of transition, the benefits would be appreciable since the viscous drag of a turbulent boundary layer can be four or more times greater than that of a laminar layer. It has been found experimentally (Coustols and Savill, 1992) that passive surface textures, e.g. streamwise riblets, can reduce the *turbulent* drag on a surface by five to ten percent. We have confirmed this numerically and have shown that riblets work by damping the near-wall spanwise fluctuations (Goldstein et al., 1995, Goldstein and Tuan, 1996). However, there has been little recent effort to control or constrain the lateral spread of the late stages of natural or bypass transition by such passive texturing. There appears to be a unique opportunity here: surface textures like riblets have not seen wide application due to their relatively modest benefits in reducing turbulent drag. Locally, however, where the flow is transitioning, there is such a large change in surface shear stress that riblets might find use if they can be optimized to delay or constrain such transition.

Related issue of roughness-induced transition: Since 2001, a series of AFOSR-sponsored experiments by Dr. Ed White (now at Texas A&M) has explored how spanwise arrays of 3D roughness elements generate transient disturbances and the circumstances under which these disturbances lead to transition. Briefly, the experiments have found that roughness-induced disturbances do indeed generate steady disturbances that undergo transient growth. However, the growth observed in the experiments is not well predicted by optimal disturbance theories because the near-field details associated with boundary-layer flow over the roughness are not captured by the theories (White 2002, 2005).

The Force Field Model and Spectral Approach: We have a method for modeling a variety of surfaces in a spectral method simulation (Goldstein et al., 1993,1995, Goldstein and Tuan, 1996). The spectral code we use is based on the method in Kim, Moin and Moser (1987). The geometry of interest here is a developing boundary layer in a channel that has a texture (roughness or riblets) on one wall. The spatial development in the normally homogeneous streamwise direction is modeled, as in Goldstein et al (2001), via an absorbing buffer zone. Figures 1 and 2 illustrate the domain used to examine turbulent spots over riblets and a sample turbulent spot.

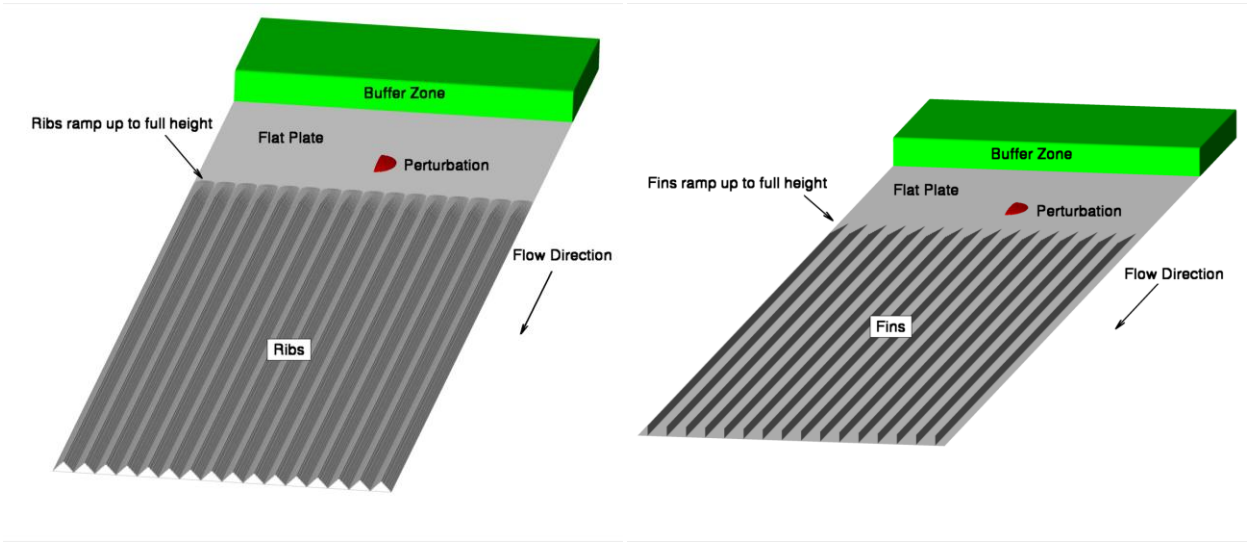

Figure 1 – Schematic of riblet surface (left) and fin surface (right), also showing the buffer zone and the location of the perturbation.

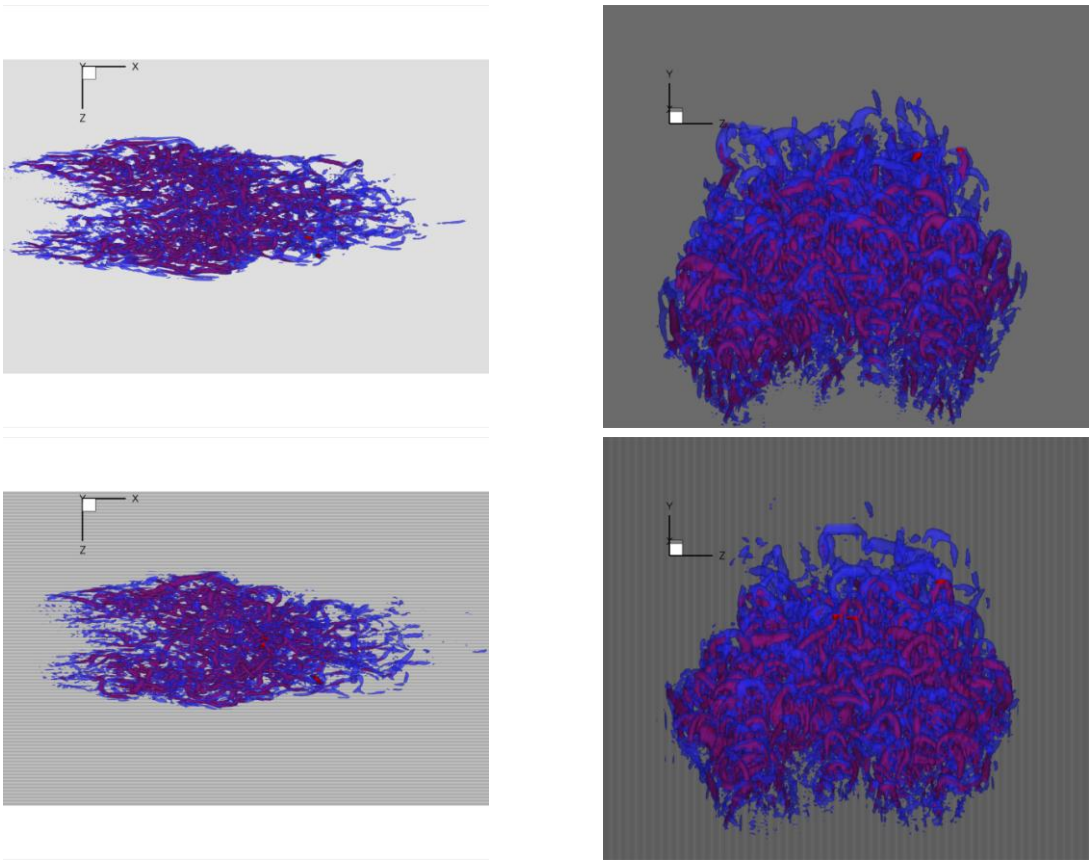

Figure 2 – Turbulent spot over a flat wall (top row) and streamwise riblets (bottom row), shown with two isosurfaces of λ_2. The surface at -0.0044 $(U_\infty/\delta_o^*)^2$ is translucent, to allow the surface at -0.0088 $(U_\infty/\delta_o^*)^2$ to be seen. Left image is a top-down view, right image shows the spot from the rear in oblique perspective. U_∞ is the freestream velocity and δ_o^* is the laminar boundary layer displacement thickness at the location of the perturbation. Riblet height and crest to

crest spacing are 0.53 δ_o^* and 1.11 δ_o^*. This run used 512×64×512 spectral modes in the x, y, and z directions, respectively.

Effort Under This Grant

Surface Textures to Control the Growth of Turbulent Spots: We have concentrated on elucidating the mechanisms of lateral spreading of turbulent spots over different surfaces and using different analytical tools. We detail some of the results below.

Flat plate

The spot over a flat plate will serve as the baseline for comparison. The domain used for these simulations had dimensions of 93 δ_0, 7.4 δ_0, and 37.0 δ_0 in the streamwise (x), wall-normal (y), and spanwise (z) directions respectively, and δ_0 is the velocity boundary layer thickness at the location of the perturbation. The computational domain has 256x128x512 spectral modes in the x,y, and z directions respectively.

Figure 3 below depicts a turbulent spot at t=13.5 δ_0/U_∞. The viewer is facing downstream about 55 degrees above the horizontal. This is a plot of an iso-surface of swirling strength, λ_2, as proposed by Jeong and Hussain and colored by distance above the plate surface. The turbulent spot has evolved into the characteristic arrowhead shape with a significant number of hairpins as well as quasi-streamwise vortices.

The evolution of one quasi-streamwise vortex on the left wingtip is shown in Figure 4. Understanding the evolution of quasi-streamwise vortices is important since they are often the precursor to hairpin structures. If the formation of quasi-streamwise vortices can be interfered with, then maybe spanwise spreading of spots can be reduced.

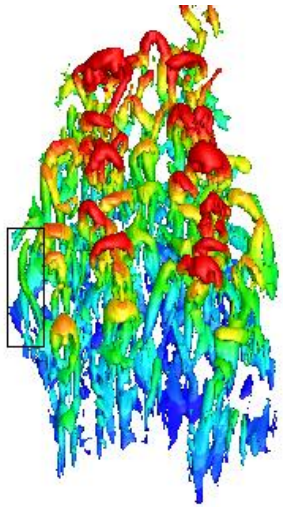

Figure 3 – Turbulent spot over a flat plate. Viewer is facing downstream about 55 degrees above the horizon.

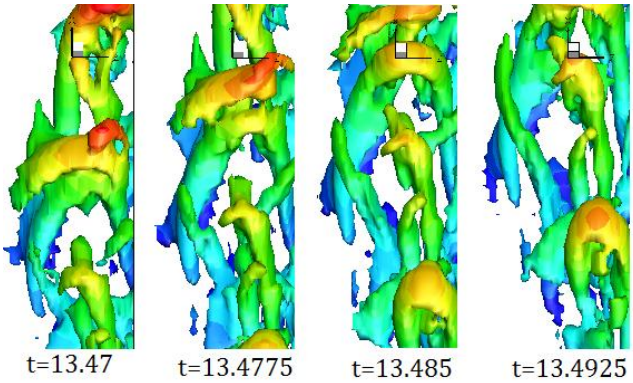

Figure 4 – Formation of a quasi-streamwise vortex on the left wingtip of the spot.

Prodding the Spot

To isolate the cause of spanwise spreading, several non-physical experiments were conducted.

Removing Middle of the Spot

To isolate the origin of spanwise spreading, we first used closely spaced damping fins to damp out the turbulence in the center of the spot and see the effect on spanwise spreading. Spanwise damping fins force spanwise velocity to zero (but do not directly affect the other two velocity components) and previous research found that spanwise damping fins can effectively remove turbulence. If the turbulence *at the center of the spot* is a major contributor to spanwise spreading, then damping out the center should dramatically decrease the spanwise spreading rate. Figure 5 shows the progression of the turbulent spot at $t = 15\ \delta_0/U_\infty$, $t = 26.25\ \delta_0/U_\infty$, and $t = 37.50\ \delta_0/U_\infty$. From top to bottom, the figures are flow with no damping fins, half spot width of damping fins, and ¾ spot width of damping fins. These are contour plots of enstrophy.

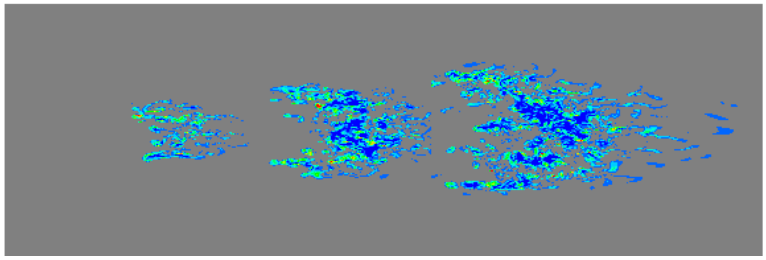

Spot over ordinary flat surface

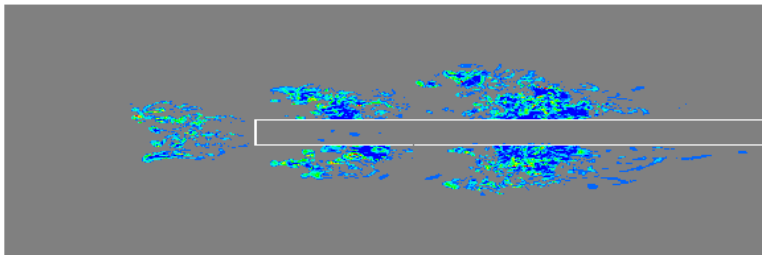

Spot passing over a wedge of damping fins approximately half spot wide.

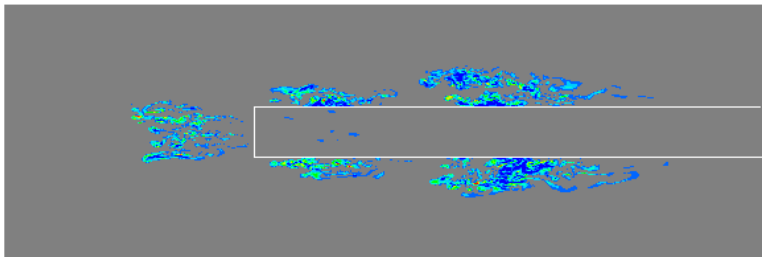

Spot passing over a wedge of damping fins approximately ¾ spot wide.

Figure 5 – Comparison of spot growth with the turbulent center of the spot damped out with damping fins as plots of enstrophy contours. Top plot has no damping (same as a flat wall case). Middle plot has about half of the spot damped out using damping fins. Bottom plot has 3/4 of spot damped out using damping fins.

Even in the extreme third case of removing a majority of the spot, it continues to spread more or less unimpeded. This suggests that the spreading mechanism is localized in the wings of the spot and is not due to some influence of the core of the spot propagating outwards.

Damping Fins

Strand and Goldstein found that spanwise damping fins are extremely effective in controlling the spanwise spreading of turbulent spot. We thus began a small parametric study to examine damping fins of height 0.186 δ_0, 0.372 δ_0, 0.744 δ_0, and 1.116 δ_0 to determine the critical height in which spots are affected. Figure 6 is a time elapsed view of the spot with damping fin height of 0.74 δ_0 and spacing of 1.15 δ_0. The iso-surfaces of the spots at four different times are overlapped in one image. Figure 6 clearly shows that damping fins with height of 0.74 δ_0 can completely stop spanwise spreading without damping out the spot. The streamwise vortical structures such as the legs of the hairpin vortices and streamwise vortical tubes are completely 'trapped' between the damping fins while the heads of the hairpin vortices stick up above the fins.

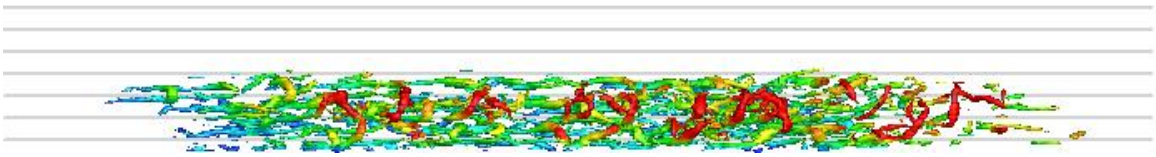

Figure 6. Time elapsed top view of the spot with damping fins of height 0.74 δ_0. The flow is from left to right. Spot is shown with iso-surfaces of swirling strength colored by distance above the plate. Spanwise spreading is completely halted by the damping fins.

Figure 7 below shows the side view of one turbulent spot. The translucent grey region indicates the height of the damping fin. Damping fins of half this size can also significantly reduce spreading angles, but not completely trap the turbulence. This simulation suggests that the spanwise spreading mechanism must be most significant near the wall.

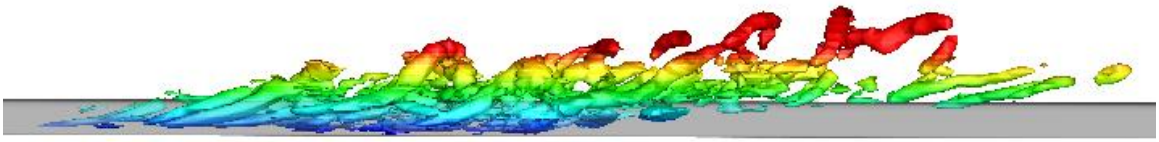

Figure 7. Profile view of a turbulent spot with iso-surface of swirling strength and colored by distance above the plate. Flow is from left to right. The gray translucent region indicates the presence of the damping fins.

In addition to affecting spreading rate, damping fins also qualitatively changed the structures of the spot. Compared to spot over flat plate in Figure 3, fewer full hairpins can be picked out from the spot over 0.372 δ_0 damping fins in Figure 8. The spot is dominated by incomplete hairpins and a few large hairpins as opposed to a 'forest' of hairpins.

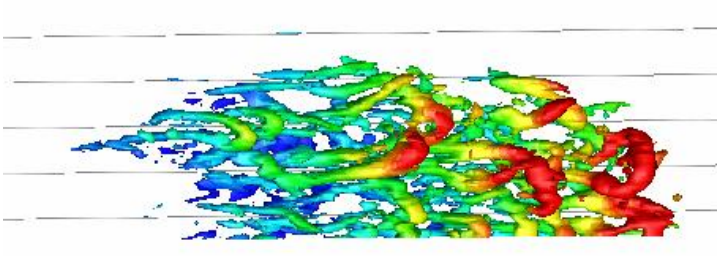

Figure 8. Top view of a turbulent spot over 0.372 δ_0 with iso-surface of swirling strength and colored by distance above the plate. Flow is from left to right. Spot centerline is on the bottom.

Spanwise Slipping Flat Plate

One proposed mechanism for self-sustaining wall turbulence involves unsteady surface separation in which a strong vortex moves near-wall fluid into an adverse pressure gradient, the fluid erupts away from the wall, and a new vortex forms in a shear layer created by the eruption. This mechanism could explain why spanwise damping fins are so successful at containing turbulent spots. To examine this supposition, we turned off the spanwise forcing term that creates the solid flat plate to allow the flow to slip and remove the shear layer on the wall. Figure 9 shows the spot at t=11.25 δ_0/U_∞. This spot is passing over a flat surface that has no slip in the streamwise direction and no through flow. But the plate does allow slip in the spanwise direction.

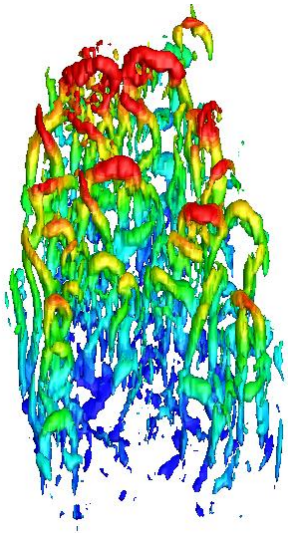

We find the result surprising. The spot looks remarkably similar to a spot over a regular flat plate. There are hairpin vortices and quasi-streamwise vortices. But these vortices cannot interact with the wall to draw out ω_x (streamwise) vorticity from the wall. The spot also spreads laterally like a typical spot over flat plate. The spanwise no-slip condition does not appear to be a factor in turbulent spot growth.

Figure 9 – Turbulent spot with spanwise slip at t=11.25 δ_0/U_∞. The viewer is facing downstream at about 55° above horizontal.

Source of Streamwise Vorticity

Our spanwise slip wall simulation showed that streamwise vorticity abounding in the spots is not shed off the bottom wall but arises from turning of the spanwise vorticity from the boundary layer shear flow. To see how and where streamwise vorticity is turned, we plotted iso-surfaces of extremely weak streamwise vorticity and very interesting structures appeared. Beyond the edge of obvious turbulence marked by coherent λ_2 structures, streamwise vorticity *layers* of alternating sign appeared. These layers are surprisingly symmetric about the spot center line even though the inner hairpins are not. Figure 10 shows the layered streamwise vorticity 'pancakes'.

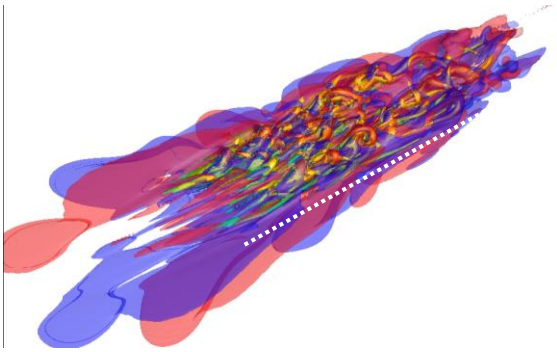

Figure 10. Turbulent spot at t = 48.9 δ_0/U_∞. Visualized by iso-surfaces of swirling strength surface (green) and iso-surfaces of weak $\pm\omega_x$ (red and blue). Flow is to upper right. Black line represents the cutting plane for Figure 16.

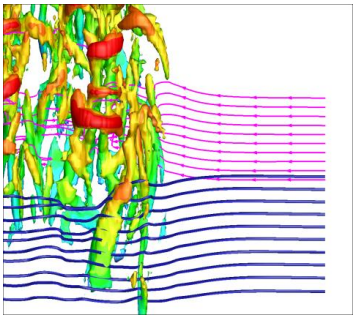

Figure 11. Top view of the right wing tip of the spot. Red and blue vortex lines show that spanwise vorticity is turned in alternating streamwise direction. Blue lines are farther above the wall than the pink lines.

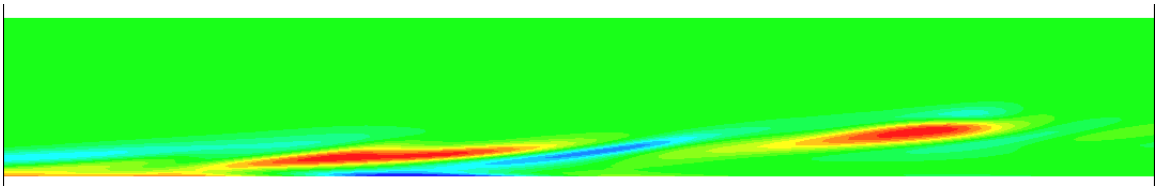

Figure 12 - Streamwise vorticity contours in the XY plane cutting through the 'pancakes'. Cutting plane shown as the white dashed line in Fig. 10.

Figure 12 shows the streamwise vorticity contour cutting through the 'pancakes'. It shows the layered structure that is inclined relative to the wall. As the spot grows downstream, old layers decay and new layers form. Figure 13 shows evidence of spanwise vorticity being turned in the streamwise direction. Some vortex lines are turned forward (producing positive streamwise vorticity) outboard of the λ_2 tubes while some are turned backward (producing negative streamwise vorticity). It is not clear, however, why these ω_x pancakes take on this alternating layer form.

Figuring out how new vortices are formed is key to understanding how the spots spread. Since newly generated vortices are predominantly streamwise, the essential dynamics of vortex formation are those of ω_x, whose inviscid evolution is governed by

$$\frac{\partial \omega_x}{\partial t} = \underbrace{-u\frac{\partial \omega_x}{\partial x} - v\frac{\partial \omega_x}{\partial y} - w\frac{\partial \omega_x}{\partial z}}_{\text{Self Induction}} + \underbrace{\omega_x \frac{\partial u}{\partial x}}_{\text{Stretching}} + \underbrace{\frac{\partial v}{\partial x}\frac{\partial u}{\partial z} - \frac{\partial w}{\partial x}\frac{\partial u}{\partial y}}_{\text{Tilting}} \qquad (9)$$

Inside the boundary layer, the second half of the tilting term, $-(\partial w/\partial x)(\partial u/\partial y)$ dominates the tilting term due to the $\partial u/\partial y$ term. The production of streamwise vorticity by self-induction, stretching, and tilting in a turbulent spot is examined. Figure 13 below shows the distribution of ω_x production at the right wingtip of a spot.

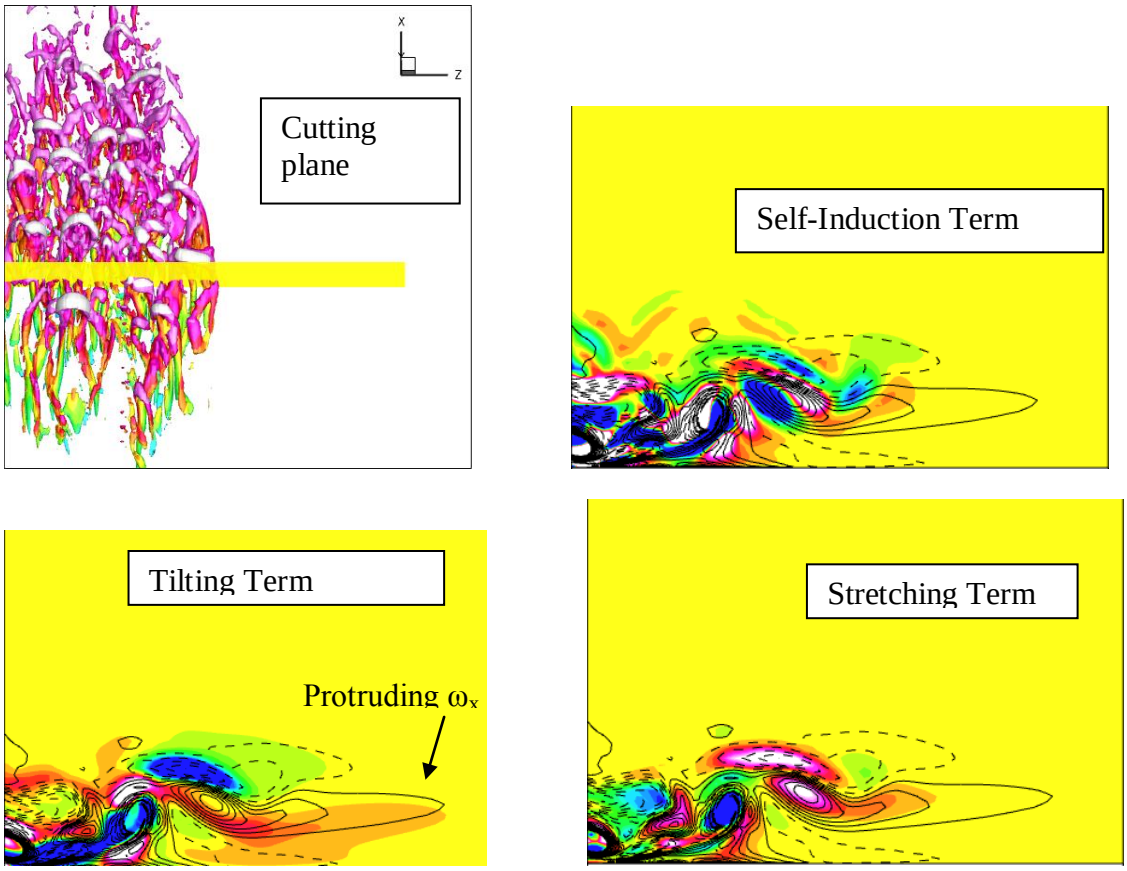

Figure 13. Distribution of selected terms of the ω_x evolution equation near spot wing tip. Visualized by contours of given term and lined by ω_x (dashed for negative). The contour levels are the same to facilitate direct comparison.

Notice that the tilting term extends farther outward than the self-induction or stretching terms. The tilting term also appears to correlate well with the ω_x layer that protrudes out of the spot.

We believe the second half of the tilting term, $-(\partial w/\partial x)(\partial u/\partial y)$, is responsible for the existence of the ω_x 'pancakes'. At the edge of spot, one can easily find tilted quasi-streamwise vortices either as the legs of hairpins, or independent quasi-streamwise vortices (see Fig. 7). An ω_x vortex induces rotating fluid motion which produces positive and negative spanwise velocity above and below the vortex (see Fig. 14 and 15).

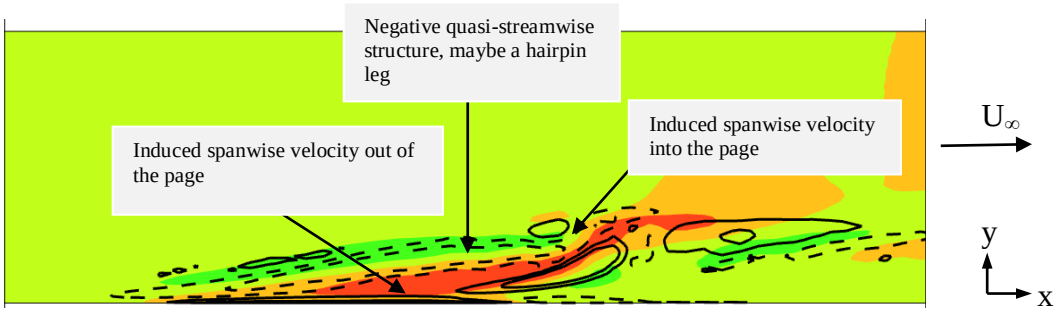

Figure 14. Spanwise velocity around a quasi-streamwise vortex. Contour flooded by spanwise velocity and lined by ωx (dashed line for negative). Flow is from right to left.

Then due to the natural inclination of the vortex, $\partial w/\partial x$ exists since the spanwise velocity goes from positive to negative as x increases in this particular instance. Figure 15 shows contours of $\partial w/\partial x$, which are particularly strong at locations where the vortex is more inclined. Then second half of the tilting term $-(\partial w/\partial x)(\partial u/\partial y)$ can thus be produced by the combination of inclined quasi-streamwise vortices at the spot wingtip and the boundary layer shear.

Figure 15. $\partial w/\partial x$ around a quasi-streamwise vortex. Contour flooded by $\partial w/\partial x$ and lined by ω_x (dashed for negative).

Several clues from our simulations suggest that the second tilting term $-(\partial w/\partial x)(\partial u/\partial y)$ is an important factor in spot spanwise spreading. It is the only term in the streamwise vorticity evolution equation that transfers base shear, $\partial u/\partial y$, from the boundary layer into streamwise vorticity. Spanwise damping fins, which are extremely effective in constraining the spot spanwise growth, completely kill the tilting term by zeroing $\partial w/\partial x$ below a critical height in near wall regions. The vortices above the damping fins may not spread because the contribution from the $\partial u/\partial y$ term is small. In the spanwise-slip wall case, the $\partial w/\partial x$ would be larger than the no-slip case near the wall. This could explain the elongated size of the spot.

Conclusions Concerning Spots

We learned several things about the turbulent spot spreading mechanism by simulating spot growth over surface textures. (I) The turbulent spot spanwise spreading mechanism is localized at the spot wing tips very close to the wall. (II) The spot can spread regardless of the flow condition at the center of the spot. By adjusting the amount of spanwise slip on the bottom wall, we learned that (III) the spanwise no-slip condition is a factor in hairpin and streamwise vortex growth and decay, but does not appear to be a factor in spot spanwise growth. Spots continue to spread even with a spanwise slip wall, which indicates that (IV) streamwise vorticity created at the edge of spots is not shed off the bottom wall; instead it originates from turning of spanwise vorticity. Extracting kinetic energy from the bottom wall using partial slip wall does not significantly alter lateral spot growth. Analysis of the inviscid streamwise vorticity evolution equation suggests that inclined streamwise vortex structures appear responsible for the production of alternating layers of streamwise vorticity observed at the spot edge.

The above work on examining the mechanisms of spot spreading was presented in a paper at the 2010 AIAA Orlando meeting with lead author Jeff Chu. Our earlier work on how to

accurately measure spreading rates and proving that real riblets can reduce spreading has recently appeared in papers in *J. Fluid Mechanics* and the *International Journal of Flow Control* with lead author James Strand. James has switched over the PECOS project and Jeff took over the project from James. Jeff is a winner of a Thrust 2000 award for academic excellence. He has now passed both his written and oral qualifying exams. Jeff has recently made a substantial effort to speed up the spectral code and took Bill Saric's stability and transition class.

Understanding boundary layer transition caused by roughness: Collaborative work with Ed White. Since August 2008, we have been trying to reconcile simulations and experiments on laminar boundary layer perturbations and transition caused by an array of hockey-puck shaped roughness elements. Ed and his students have done detailed wake surveys of such roughness in preparation for studies of his periodic roughness tiles. Don Rizetta and Miguel Visbal have done DNS matched to Ed's experiments. Although they do not have a perfect match, their results compared rather well. To check our processes in our own DNS, we too tried to match those previous results. Our results match the previous two data sets very closely when we use sufficient spatial resolution to have smooth cylindrical shapes represented in the DNS. To confirm flow structural details not available from the previous work, we also performed a set of flow visualization experiments in our water channel and used a high resolution LDA survey behind the roughness elements. Finally, we have begun simulations to match the TAMU experiments on subcritical flow over quasi-random patches of roughness. Whereas the hotwire experiments only currently measure the wake behind the patches, with DNS we obtain the complete flow field and can trace where the features observed with the hotwires originate. We summarize our efforts below.

The focus of this work is the transient growth of boundary layer disturbances induced by roughness on a flat plate. Disturbances produced, and their involvement with the onset of transition, had previously been found to be partly dependent on the roughness height based Reynolds number, Re_k. Periodic arrays of circular cylinders are used to perturb low Mach number flows in matched experimental and computational efforts.

Our work (with student C. J. Doolittle who took over from Kelly Stephani) started with a sub-critical simulation at a Re_k of 50 with the intention of gaining confidence for further studies. The DNS code used was again the spectral method that uses an immersed boundary approach for simulation of both the cylindrical roughness element as well as the underlying flat plate. Adjustments were made within the main code to properly develop a Blasius boundary layer before roughness was introduced. These included changes to the "suction wall," a layer of forcing cells used to correct for pressure gradients within the computational domain, and the "buffer zone," an upstream region which mitigates inflow disturbances and sets up the desired Blasius profile. The spectral method allowed for the quick development of steady boundary layer flow within a much smaller spanwise domain, which in turn was then copied and stitched into the desired

space. Figure 16 shows an example comparison between the resulting undisturbed DNS Blasius boundary layer and an analytical representation.

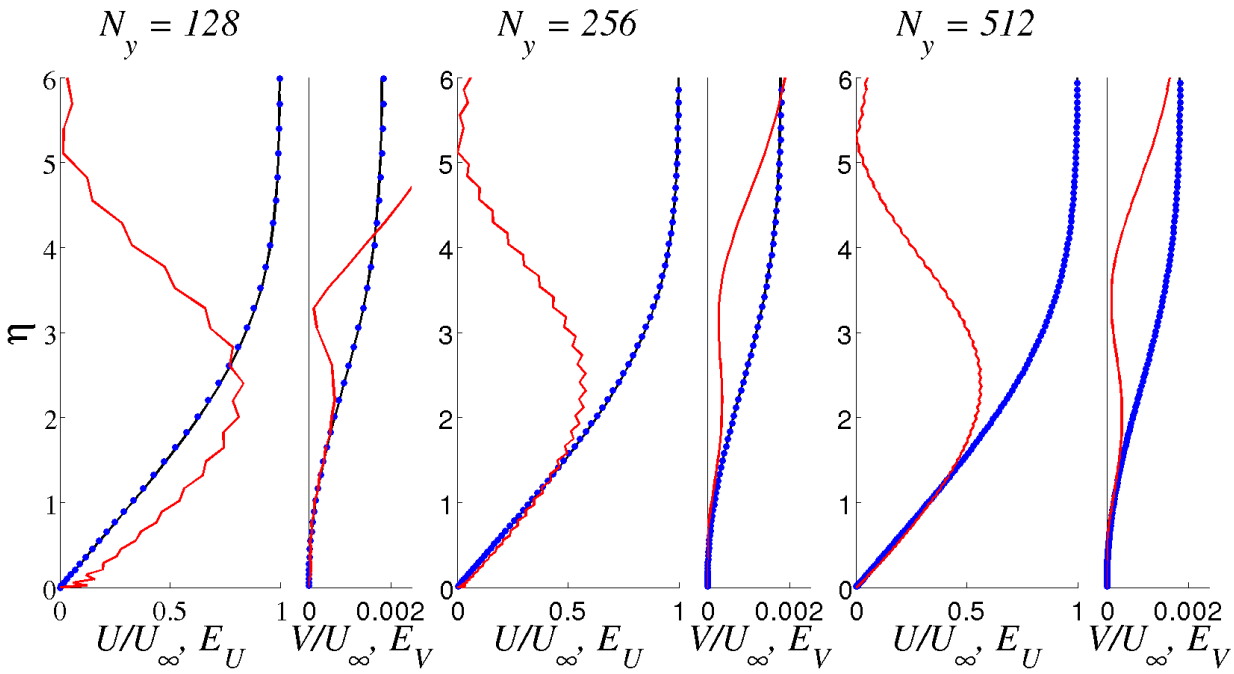

Figure 16: Boundary layer profiles for three different grid resolutions prior to introducing cylinder. DNS results for nondimensionalized streamwise and 100x wall-normal velocities (blue) are plotted with solutions to the Blasius equation for flat-plate flow (black). Percent error for both velocities (red) show negligible error.

Results of this preliminary study showed expected flow properties of a sub-critical roughness case. Two dimensional data sets corresponding to multiple downstream locations were extracted for examination by the research group at Texas A&M University. Data from the Re_k = 50 simulation as well as previously found results of Stephani and Goldstein at another sub-critical Re_k of 202 were brought to Texas A&M University for analysis by C. J. during a brief student exchange. Biorthogonal decomposition was performed to obtain the continuous spectrum distribution and compared with prior DNS results of Rizzetta and Visbal for the 202 case. Similar results were found using a newly developed decomposition approach which does not require the pressure field.

Stephani and Goldstein (2009) noted discrepancies between their DNS results and those of Rizzetta and Visbal as well as the experimental results of Ergin and White. Streamwise velocity contours in the near wake displayed interesting flow structure consisting of small humps within the disturbance field (Figure 17). With respect to the experimental findings this difference appeared to be due to a lack of spanwise resolution due to the width of the hot-wire used. Spanwise filtering was performed on DNS data resulting in very similar findings between our DNS and Ergin and White's experiments. Discrepancies between the two DNS simulations were suspected of being caused by the number of upstream collar vortices predicted by either code. Stephani and Goldstein

found four such collar vortices draped about the cylinder and suggested that the strongest three of these directly influence the near wake flow disturbance field. Rizzetta and Visbal on the other hand found only two collar vortices which led to results that look similar to the experimental findings of White but without accounting for the experimental sampling grid and hotwire width (Figure 18).

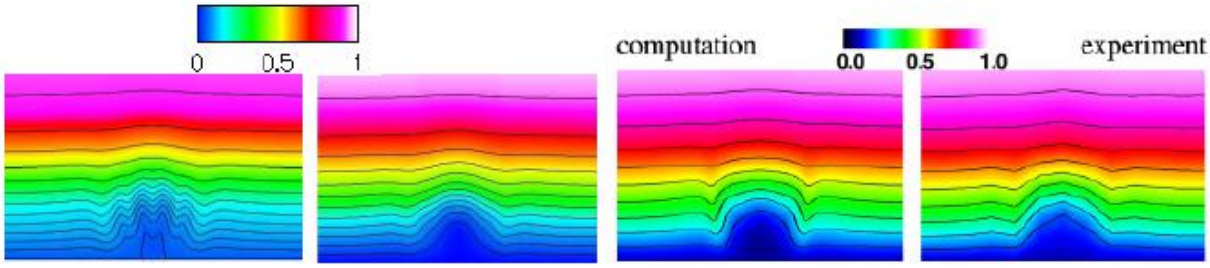

Figure 17: Streamwise velocity contours taken at about 1.5 cylinder diameters downstream. From left to right: Stephani and Goldstein DNS; Stephani and Goldstein DNS filtered onto the Ergin and White grid; Rizzetta and Visbal DNS; Ergin and White hot-wire. Note the "humps" in Stephani and Goldstein's unfiltered data. Results match experimental data fairly well after filtering which is why spanwise resolution of the hot-wire study was questioned.

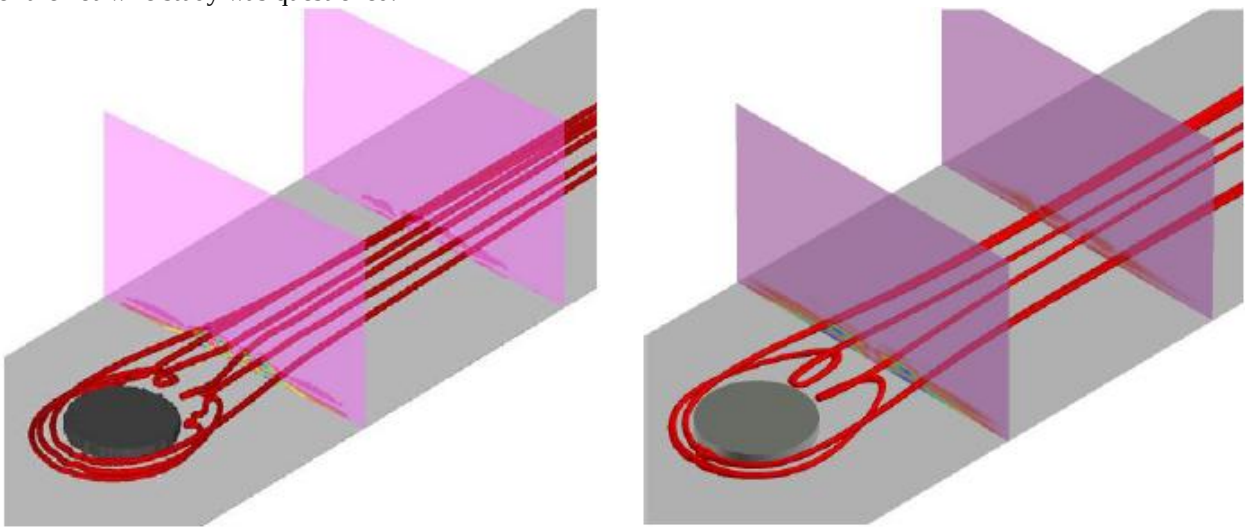

Figure 18: Our DNS results (left) and Rizzetta and Visbal (right). Streamtubes initiated at the cores of the upstream collar vortices are displayed in red. Our simulation found three primary vortices where as Rizzetta and Visbal only found two.

These findings led to a new set of experimental and computational studies with the intention of sorting out the differences. Laser Doppler Anemometry was used along with flow visualization in the UT water channel to compare directly with experimental results.

Geometrical and flow properties were scaled appropriately for water channel analysis. Unfortunately, the scaled spanwise resolution of the LDA system used (a spot size of about 3mm using our 400mm lens) was no better than that of the Ergin and White hot-wire experiments. As such, the flow structure downstream of our cylindrical roughness element was very similar to those previous experimental findings. We have since purchased a beam expander to increase the spanwise resolution of the LDA system.

The results can be seen in figure 19. In the leftmost subfigure are high resolution LDA wake profiles which clearly agree with the Rizzetta and Visbal (RV) DNS and the EW hotwire results (given that there is horizontal smoothing of the hotwire data due to the width of the wire). These new data were presented in the Orlando 2011 ASM meeting by new student Scott Drews who took over after C. J. Doolittle graduated. Scott has also obtained the center figure which is a not quite settled DNS result on a much finer grid. (Settled results look even better.) One clearly sees that the extra humps in the profile are missing. Those humps were caused by the shear layer over the top of the roughness element splitting as it passed over the trailing edge of the element if that edge was not smooth.

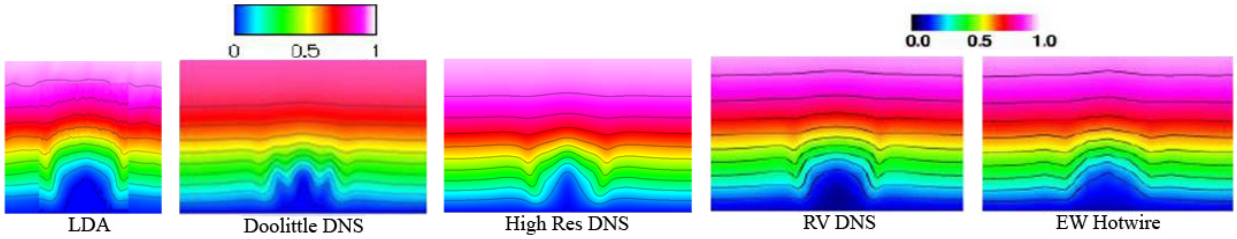

Fig 19. Comparison of streamwise velocity contours on streamwise normal slices 1.5 diameters downstream of the aft edge of the element. Left figure is LDA experiments in water tunnel, middle 3 figures are DNS from Doolittle, current high resolution DNS, and Rizzetta and Visbal[3], and right figure is hotwire experiment of Ergin and White. Note that vertical stretching is used to highlight the differences between the images.

For a long time we assumed that the wake structure is due to the collar vortices from ahead of the cylinder twisting and stretching and turning in the wake. We were surprised, however, to find that those vortex cores, clearly visible and rotating upstream, essentially stop rotating and become passive streamlines as they are swept around the front part of the cylinder. This appears to occur because the cores pass into lateral displacement boundary layers beside the cylinder as seen in figure 20. In that figure, the velocity vectors in stream-normal planes indicate the lateral flow whilst the colors indicate the streamwise vorticity. The stream ribbons are colored by the vorticity component along the direction of the ribbon. The upshot of such an image is that the vorticity ultimately pointing downstream in the wake upon which subsequent unsteady perturbations grow, is not upstream spanwise vorticity turned downstream but rather vorticity caused by the top of the perturbation projecting a no-slip surface up into higher speed flow. To what extent this is a low Reynolds number or particular perturbation shape effect remains to be seen. In the figures below related to the random roughness, it appears as though the tallest regions of roughness are responsible for the largest perturbations. But to what extent they are turning rather than generating fresh vorticity remains an open question.

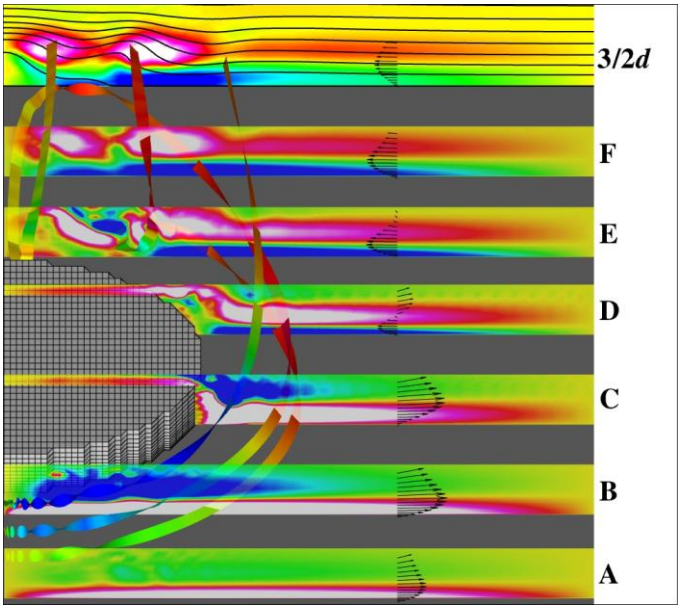

Fig. 20. Perspective view of flow about cylindrical perturbation element. Stream ribbons are initiated in the cores of the upstream collar vortices and are colored by the vorticity component along the ribbon. Colors of cutting planes are streamwise vorticity. Line contours in last plane are streamwise velocity. Velocity vectors show lateral flow in cutting planes.

Our DNS results continue to show three distinct collar vortices in the flow (figure 20) whereas Rizzetta and Visbal found only two. Using dye injection it is clear that three collar vortices are present. Figure 21 is a comparison to DNS of photographs from the water channel showing the three vortices in different colors. The right image of figure 21 is created from analyzing several photographs of each single collar vortex. Due to limitations in the dye port configuration, separate dye colors cannot be injected into the individual cores. Instead, each of the three cores is identified separately by manipulating the flow of the dye out of the bottom of the plate. Once all three cores are observed independently of each other, one can photograph all three together (left image). This image is then altered in Adobe Photoshop to create the image on the right. Each individual collar vortex is colored to help distinguish the three, and the overall composite image is compared side by side to the DNS.

The left and right comparison images in figure 21 of the *primary* (green) flow viz. cores show excellent agreement with the DNS. The images also show slightly different standoff distances for the *primary* and *secondary* (blue) vortex cores. This may be due to the blunt leading edge of the cylinder used in DNS causing an alignment issue with the photograph from the water channel. The turn locations of the *secondary* core downstream of the cylinders agree well, while the turn locations of the *tertiary* (red) cores have a small inconsistency.

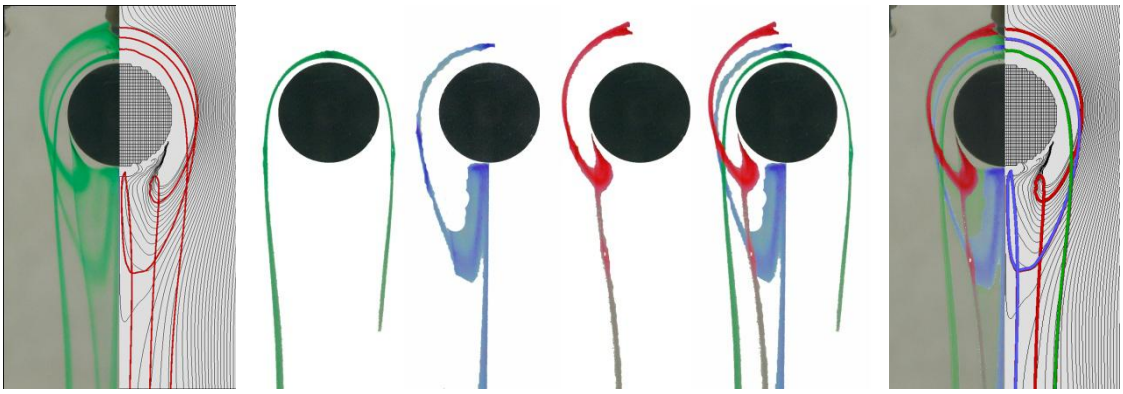

Fig 21. Buildup of water channel flow visualization and comparison to DNS results. Left figure is original image from the water channel, right image is after filtering vortices by color.

We are currently examining flow over discrete roughness patches to match the TAMU experiments. The quasi-random distributed roughness used by Downs et al. is modeled using the immersed boundary technique. Figure 22 shows a side by side comparison of the roughness patch used in experiments and the simulated roughness patch used in DNS. The figure suggests that the immersed boundary is reasonably capable of modeling the experimental roughness patch. Due to differences between the rapid-prototyping process used by Downs et al. and the immersed boundary technique, the experimental roughness has slightly rounded corners whereas the immersed boundary technique creates a set of plateaus. However, high order (x,z) filtering of the force field used in the spectral DNS will slightly smooth those corners as well. The experiments are conducted using five distinct patches of roughness (only two of which are shown in figure 22). This is done to average the velocities across all five patches to reduce noise. The DNS is truly periodic: only one patch is used and flow that leaves one side in the homogenous z direction of the domain is inserted on the other side.

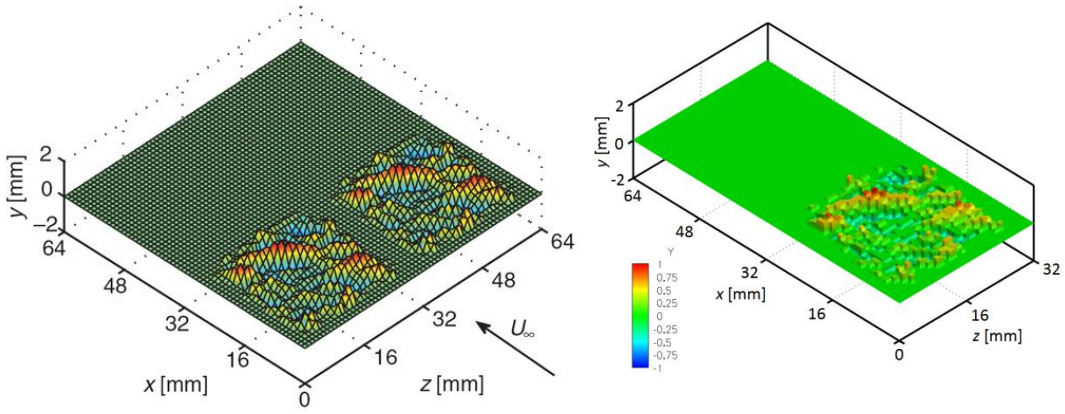

Fig 22. Left image is a pair quasi-random distributed roughness patches from Downs et al.[6] representing input to the 3D printing machining process. Right image is a single roughness patch used in current DNS. Note vertical stretching used for clarity.

To compare the DNS data to experimental data of Downs et al, three simulations are run for the corresponding freestream speeds of 7.5, 9.3, and 11.5 m/s. Due to the nature

of the cosine grid in the wall normal direction, matching the incoming Blasius profile of experiments leads to height based Reynolds numbers (Re_k) values of 174, 237, and 311. The Re_k values for DNS are off by ~10 from the experimental Re_k values of 164, 227, and 301 due to the small error in roughness patch height.

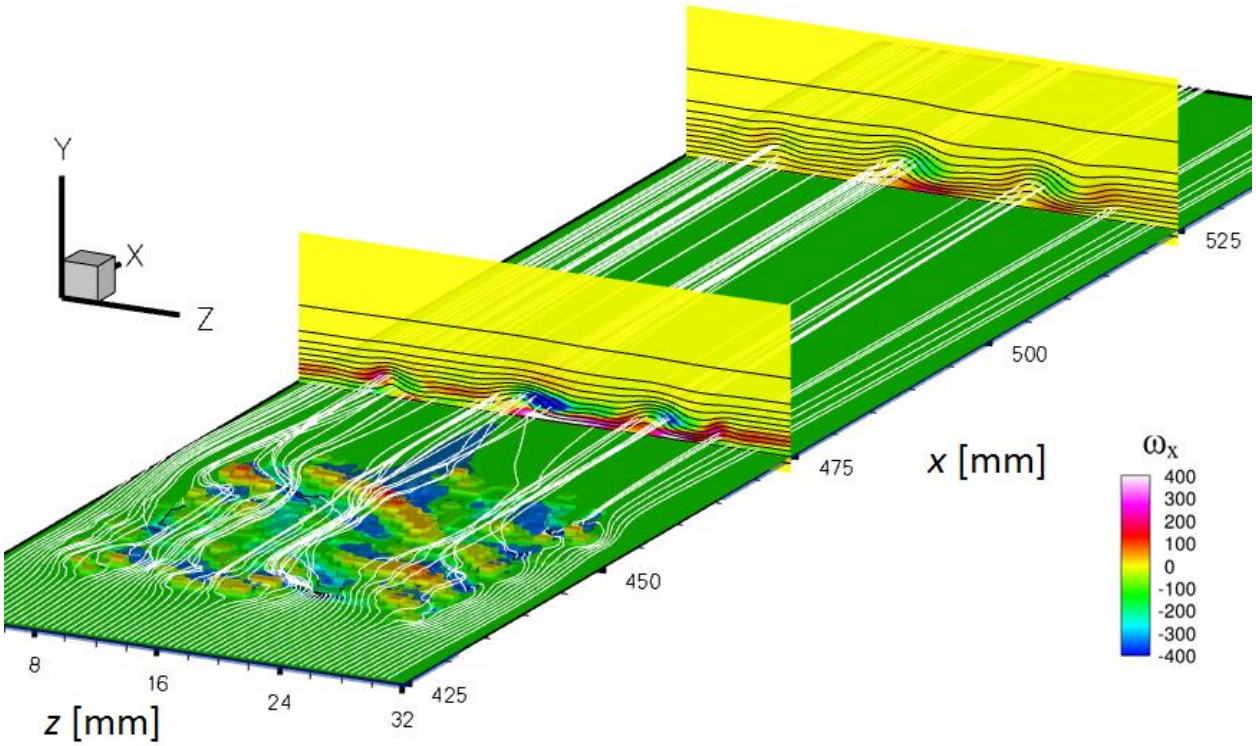

Fig 23. Flow field for Re_k = 237 over roughness patch. Downstream slices colored by streamwise vorticity and contoured by 10% velocity increments. Negative (*u*-) velocities are shown by a blue isosurface.

Figure 23 illustrates flow over the roughness patch run in the DNS code. The stream-normal slices are colored by streamwise vorticity with contour lines of 10% velocity increments. As the figure shows, the streamlines, generated from a spanwise rake upstream of the roughness patch, coalesce around areas of higher magnitude vorticity, corresponding to a velocity deficit. As the wall normal height of the rake increases, the streamlines become less perturbed and tend not to coalesce as much. At a wall normal height of 1.5 mm, the streamlines are relatively unperturbed with only a few streamlines coming together. The three regions of tall roughness, colored in red, have similar effects on the flow. Behind each of these three regions, a velocity deficit develops, as well as an area of large magnitude streamwise vorticity. The area of large positive streamwise vorticity at the wall (colored in white at x=475 mm, z=16 mm) is due to the shear created by the large negative vorticity created behind the tallest region of the roughness. The leftmost velocity deficit (x=475 mm, z=6 mm) region is created by a pair of counter rotating vortices, however the other two velocity deficit regions (x=475 mm, z=14 mm and 23 mm, respectively) are each created by a dominant single clockwise vortex. The counter rotating vortices are created because the roughness is more like a discrete, symmetrical element at z=6 mm, whereas the single vortex cores at z=14 mm

and 23 mm are created because the roughness that creates them is more of a ridge-like discrete asymmetric element at an angle to the flow. The white regions in the z=14 mm and 23 mm are created by the negative vortices drawing up the flow on the wall. The second stream-normal slice at x=525 mm is very much like the first except that the streamwise vorticity has diffused. The vortex cores were not, in fact, all that strong and cause little net rotation between the two slices (e.g., the relative locations of the positive and negative cores is essentially unchanged).

Streamwise velocity contours downstream of the roughness patch are shown in figure 24 for locations of 475, 525, and 600 mm downstream of the leading edge of the flat plate. The DNS and experimental results compare well and show essentially the same flow. Each downstream slice shows three clear velocity deficit regions, corresponding to the coalescence of the streamlines near those spanwise locations. As the downstream slice location is moved further aft of the roughness patch, the disturbances closer to the wall dissipate, while those further from the wall increase in magnitude. The velocity deficit regions may be less pronounced for the experimental results due to a filtering effect created by the hotwire. Because the hotwire has a finite width, the data are filtered or smoothed over a finite spanwise extent, lessening the severity of the velocity deficit peaks.

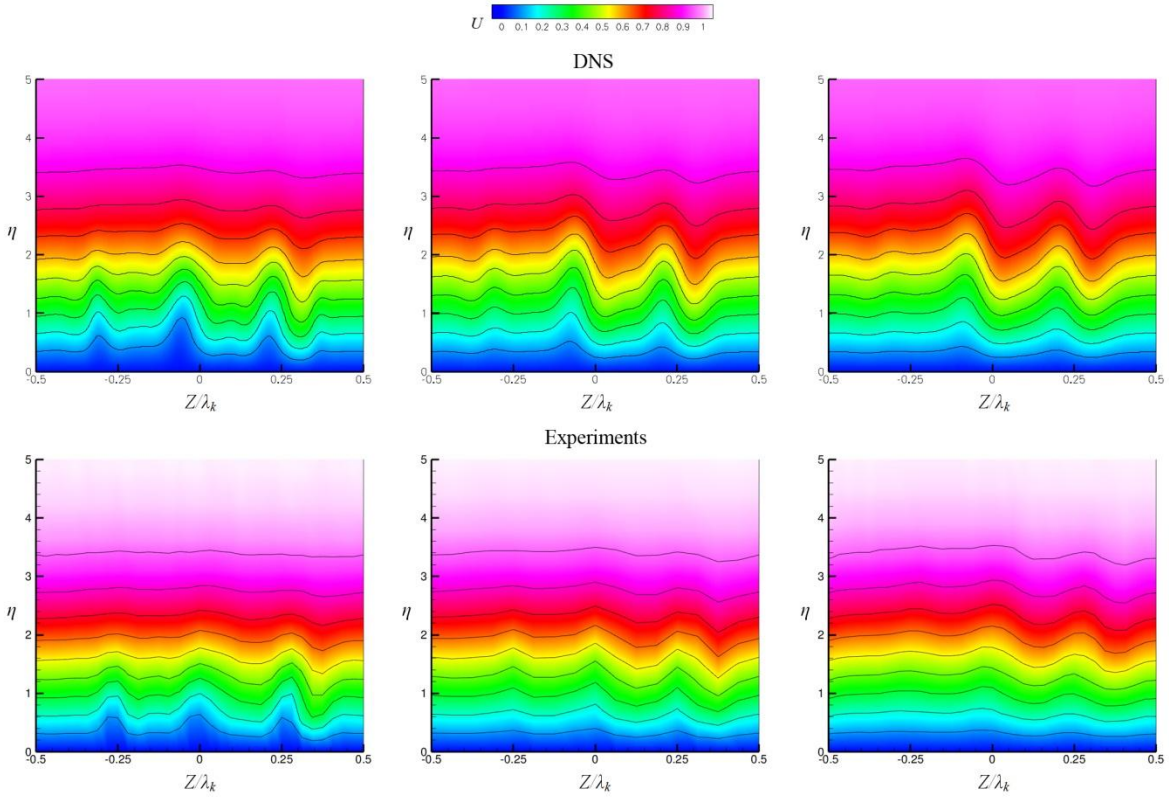

Fig 24. Velocity contours for Re_k = 164/174 at downstream locations of 475, 525, and 600 mm from the leading edge of the flat plate. Top images are from current DNS, bottom images are from Downs et al.

For the flow-over-roughness work, Scott Drews took over after C. J. Doolittle (who graduated) who had taken over from Kelly Stephani who switched over to a NASA NRA hypersonics project. C. J. and Kelly were also winners of Thrust 2000 awards. Results from this work were separately presented at AIAA meetings with lead authors Kelly and Scott, at a APS-DFD meeting by C. J. and have been submitted to AIAA Journal by C. J.. We have had several exchange visits between the UT and A&M groups and the collaboration is continuing.

References:

E. Coustols and A. M. Savill, 1992, Special course on skin-friction drag reduction, p. 8-1 to 8-55, March 2-6, in AGARD Report 768.

M. Gad-El-Hak, R. F. Blackwelder, J. J. Riley, "On the growth of turbulent regions in laminar boundary layers," *J. Fluid Mechanics*, Vol. 110, 1981, pp. 73-95.

D. B. Goldstein, R. Handler, and L. Sirovich, 1993, *J. Comp. Phys*., **105**, pp. 354-366, and 1995, *J. Fluid Mech.*, **302**, Nov. 10, 333-376.

D. B. Goldstein and T.-C. Tuan, 1996, *J. Fluid Mech*., **363**, pp. 115-151.

D. B. Goldstein, J. Cohen and V. Levinski, 2001, 3rd AFOSR Int. Conf. on DNS and LES

Henningson, D., Spalart, P. & Kim, J., 1987, *Phys. Fluids* **30** (10) October.

R. Joslin, 1998, *Ann. Rev. Fluid Mech*., **30**, 1-29.

J. Kim, P. Moin, and R. Moser, 1987, *J. Fluid Mech*., **177**, 133.

Rizzetta, D. P. & Visbal, M. R., 2006, AIAA paper 2006-3527, presented at the 36th Fluid Dyn. Conf., San Francisco.

E. M. Saiki and S. Biringen, 1994, in *Transition, Turbulence, and Combustion Vol 1: Transition*, ed. Hussaini, M., Gatski, T. and Jackson, T., Klewer Publ., The Netherlands, p. 267-276.

E. M. Saiki and S. Biringen, 1997, *J. Fluid Mechanics*, **345**, 133-164.

H. Schlichting, 1979, *Boundary Layer Theory*, 7th ed., McGraw-Hill.

B. Singer and R. Joslin, 1994, *Phys. of Fluids*, **6**, no. 11, Nov. 3724-3736.

Strand, J. S. and Goldstein, D. B. "*DNS of Surface Textures to Control the Growth of Turbulent Spots*," 45th AIAA Aerospace Sciences Meeting and Exhibit, Reno, NV, Jan. 2007

Strand, J. S. "*DNS of Surface Textures to Control the Growth of Turbulent Spots*," Master's Thesis – The University of Texas at Austin, Dec. 2007

N. Tillmark, 1995, *Europhys. Lett*, **32**, 481-485.

E.B. White, 2002, *Phys. Fluids* **14:**4429–4439.

E.B. White, J.M. Rice and F.G. Ergin. 2005, *Phys. Fluids*, **17**:064109.

J. Wygnanski, M. Sokolov and D. Friedman, 1976, *J. Fluid Mechanics*, **78**, 785-819.

Personnel Supported:

Jeff Chu – Graduate Student, UT Austin
Charles (C.J.) Doolittle – Graduate Student, UT Austin
Scott Drews _ Graduate Student, UT Austin
Kelly Stephani – Graduate Student, UT Austin
David Goldstein – Professor, UT Austin

Publications/Talks:

Stephani, K. A. and Goldstein, D. B., "DNS study of transient disturbance growth and bypass transition due to realistic roughness," paper 2009-0586 AIAA ASM Mtg., Orlando, 2009.

Stephani, K., and Goldstein, D., "DNS study of transient disturbance growth and bypass transition," Presented at the APS-DFD mtg., San Antonio, Nov. 2008.

Strand, J. and Goldstein, D., "DNS of Surface Textures to Control the Growth of Turbulent Spots", Presented at the APS-DFD mtg., San Antonio, Nov. 2008.

Strand, J. and Goldstein, D. B. "Direct numerical simulation of riblets to constrain the growth of turbulent spots," *J. Fluid Mechanics,* (2011), vol. 668, pp. 267-292.

Strand, J. and Goldstein, D. B. "Application of passive surface textures to control the growth of turbulent spots at moderately high Reynolds numbers." *Int. J. Flow Control*, vol. 2, No. 2, 2010, pp. 73-89.

Chu, J., Strand, J. and Goldstein, D., ``Investigation of turbulent spot spreading mechanism," paper 2010-0716 48th AIAA ASM Mtg., Orlando, Jan. 2010.

Strand, J and Goldstein. D., ``DNS of Surface Textures to Control the Growth of Turbulent Spots," AIAA paper 2010-915, 48th AIAA Aerospace Sciences Meeting, 4-7 January 2010, Orlando, FL.

Goldstein, D., White, E., Strand, J., Stephani, K., Chu, J, Doolittle, C. J., and Denissen, N., "Transient Boundary Layer Disturbance Growth and Bypass Transition Due to Realistic Roughness and Continued Study of Transition Over Riblets," Lecture presented at the AFOSR contractors meeting, Dallas, Nov. 2008.

Goldstein, D. "Using Immersed Boundaries to Examine Turbulent Boundary Layer Control and Laminar to Turbulent Transition," *Invited talk* at the AIAA ASM Mtg., Orlando, 2009.

Doolittle, C. J. and Goldstein, D., ``Comparing DNS and Experiments of subcritical surface roughness," Presented at APS-DFD 62nd annual Mtg., Minneapolis, Minn. Nov. 2009.

Goldstein, D. "Incompressible and hypersonic boundary layer transition over textured surfaces." Invited Lecture, Texas A & M, Jan. 28, 2010.

Goldstein, D. "Incompressible and hypersonic boundary layer transition over textured surfaces." Invited Lecture, Caltech, April 2, 2010.

Doolittle, C. J. and Goldstein, D., ``Near-Field Flow Structures About Subcritical Surface Roughness," submitted to *AIAA J.*, July, 2010.

Doolittle, C., Goldstein, D. “Parametric Study of Roughness Induced Transient Growth”. In preparation for *AIAA J*.

Drews, S., Downs, R., Doolittle, C., Goldstein, D., White, E., “ Direct numerical simulations of flow past random distributed roughness.” Paper at the AIAA ASM Mtg., Orlando, 2011.